Biochimica et Biophysica Acta 1837 (2014) 1892–1903

Contents lists available at ScienceDirect

Biochimica et Biophysica Acta

journal homepage: www.elsevier.com/locate/bbabio

High yield of secondary B-side electron transfer in mutant *Rhodobacter capsulatus* reaction centers

Lucas Kressel [a,1], Kaitlyn M. Faries [b,1], Marc J. Wander [a], Charles E. Zogzas [a], Rachel J. Mejdrich [a], Deborah K. Hanson [a], Dewey Holten [b], Philip D. Laible [a], Christine Kirmaier [b,*]

[a] Biosciences Division, Argonne National Laboratory, Argonne, IL 60439, USA
[b] Department of Chemistry, Washington University, St. Louis, MO 63130, USA

ARTICLE INFO

Article history:
Received 10 June 2014
Received in revised form 22 July 2014
Accepted 26 July 2014
Available online 1 August 2014

Keywords:
Photosynthetic reaction center
Charge recombination
High-throughput screening
Ultrafast spectroscopy
Directed evolution
Transmembrane electron transfer

ABSTRACT

From the crystal structures of reaction centers (RCs) from purple photosynthetic bacteria, two pathways for electron transfer (ET) are apparent but only one pathway (the A side) operates in the native protein-cofactor complex. Partial activation of the B-side pathway has unveiled the true inefficiencies of ET processes on that side in comparison to analogous reactions on the A side. Of significance are the relative rate constants for forward ET and the competing charge recombination reactions. On the B side, these rate constants are nearly equal for the secondary charge-separation step (ET from bacteriopheophytin to quinone), relegating the yield of this process to <50%. Herein we report efforts to optimize this step. In surveying all possible residues at position 131 in the M subunit, we discovered that when glutamic acid replaces the native valine the efficiency of the secondary ET is nearly two-fold higher than in the wild-type RC. The positive effect of M131 Glu is likely due to formation of a hydrogen bond with the ring V keto group of the B-side bacteriopheophytin leading to stabilization of the charge-separated state involving this cofactor. This change slows charge recombination by roughly a factor of two and affords the improved yield of the desired forward ET to the B-side quinone terminal acceptor.

1. Introduction

The bacterial photosynthetic reaction center (RC) is a transmembrane protein–cofactor complex that converts light energy into chemical potential for use in cellular processes. Of the three protein subunits (L, M and H), homologous L and M comprise an integral core and bind a bacteriochlorophyll (BChl) dimer (P) that is the primary electron donor, two monomeric BChls (B), two monomeric bacteriopheophytins (H) and two quinones (Q). These cofactors are arranged in two branches (A and B) in pseudo-C_2 symmetry (Fig. 1A) [1–4]. Despite the similarity between the branches, in the wild-type (WT) RC only the A-side cofactors participate in rapid multi-step electron transfer (ET) that results in nearly quantitative formation of $P^+Q_A^-$ from P* in less than a nanosecond. Subsequent $P^+Q_A^- \rightarrow P^+Q_B^-$ ET occurs on the microsecond timescale.

Site-directed mutagenesis has been used with great success over the last 25 years to explore the factors responsible for unidirectional A-side ET in the RC. Mutant RCs that perform B-side charge separation – albeit generally in low yield – have enriched our understanding of the mechanism of primary A-side charge separation and framed views of how ET from P* to the B-side cofactors is normally suppressed [5–25]. The general working model (Fig. 1B) is that the $P^+B_A^-$ state is positioned between P* and $P^+H_A^-$ supporting two initial ET steps, $P^* \rightarrow P^+B_A^- \rightarrow P^+H_A^-$, that occur on the ~0.5 to ~5 ps timescale [26–36]. On the B side, $P^* \rightarrow P^+H_B^-$ ET is much slower (~100–200 ps) with $P^+B_B^-$ thought to be higher in free energy than P* and supporting ET by a one-step superexchange mechanism. Distinctions also exist between the intrinsic properties of $P^+H_A^-$ and $P^+H_B^-$. $P^+H_A^- \rightarrow P^+Q_A^-$ ET occurs in 200 ps. In the absence of ET, $P^+H_A^-$ lives for 10–20 ns and decays by charge recombination (CR) to form the ground and triplet excited states [28,34]. In comparison, $P^+H_B^- \rightarrow P^+Q_B^-$ ET is much slower (~4 ns time constant) and $P^+H_B^-$ has a shorter intrinsic lifetime (~3 ns) [23]. This combination results in ~45% yield of $P^+H_B^- \rightarrow P^+Q_B^-$ ET compared to 100% formation of $P^+Q_A^-$ on the A side. Therefore, even if a high yield of P* conversion to $P^+H_B^-$ is achieved in a mutant, translation of that increase through to a high yield of $P^+Q_B^-$ is not assured. To achieve this end, the mutant RC would also require changes that increase the rate constant for $P^+H_B^- \rightarrow P^+Q_B^-$ ET and/or reduce the rate constant for $P^+H_B^-$ CR.

We have adopted a directed molecular evolution approach to engineering the RC to enable efficient B-branch ET that employs rapid, efficient, semi-random methods for constructing RC mutants *Rhodobacter (Rb.) capsulatus*. This is coupled to a high-throughput millisecond screening assay (ms assay) that measures the yield of $P^+Q_B^-$ formed solely via the B-branch cofactors [37]. In this work we report on two groups of mutant RCs, seeking mutations that increase the rate of $P^+H_B^- \rightarrow P^+Q_B^-$ ET and/or decrease the rates of the competing CR

* Corresponding author. Tel.: +1314-935-6480; fax: +1314-935-4481.
E-mail address: kirmaier@wustl.edu (C. Kirmaier).
[1] These two authors contributed equally to the work.

http://dx.doi.org/10.1016/j.bbabio.2014.07.015
0005-2728/

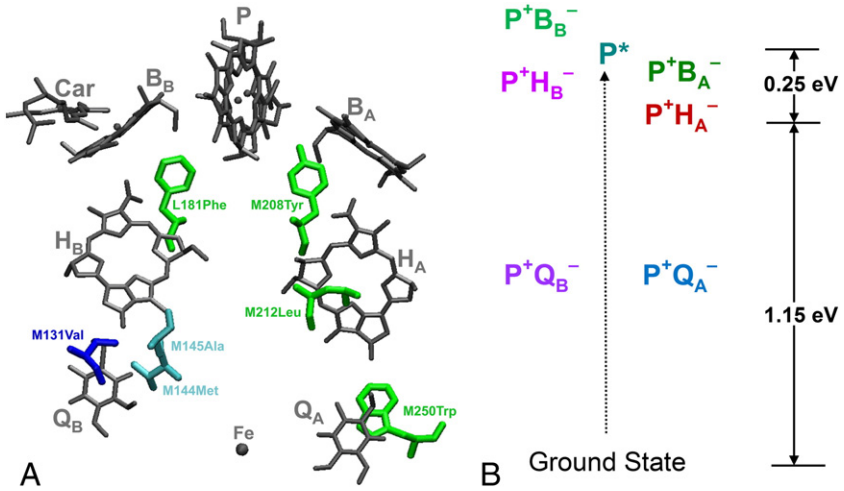

Fig. 1. (A) Positions of the substituted amino acids relative to the cofactors in the RC, from the *Rb. sphaeroides* crystal structure 1PCR [4]. Native amino acids are shown. Sites that comprise the YFHV background mutations are in green. The M131 site that was subject to extensive mutation here is in blue. The M144 and M145 sites also studied here are in cyan. See Table 1 for additional details. (B) Model free energy diagram for WT RCs.

processes of $P^+H_B^-$. The first mutant set targets residue M131 near H_B (Fig. 1A), where a Val is the native amino acid in *Rb. capsulatus* (Thr in *Rb. sphaeroides*). All amino acids were substituted at M131 ("saturation mutagenesis"), mutants denoted V(M131)X. The motivation for exploring M131 is that the C_2 symmetry-related residue on the A side is a Glu (at L104) that forms a hydrogen bond with H_A [1] and previous work has suggested that an Asp at M131 (or at M133 in *Rb. sphaeroides*) forms a hydrogen bond to H_B [10,25,38,39]. The second group couples substitution of all 20 amino acids at M131 with mutations of M144Met to Ile and M145Ala to Ser (designated "IS"). Residues M144–145 are located somewhat between H_B and Q_B (Fig. 1A) and the IS substitutions were identified by Youvan and coworkers in a photocompetent phenotypic revertant of a strain carrying multiple-site mutations in the Q_B binding pocket [40,41].

We find an increased yield of $P^+Q_B^-$ from B-side ET in RCs carrying amino acid substitutions at M131, for the IS pair alone, and for some substitutions at M131 paired with the IS mutations. Of these, five mutants were selected for further investigation of ET to and between the B-side cofactors using ultrafast transient absorption (TA) spectroscopy in order to determine the origin of improved $P^+Q_B^-$ production. Among the selected mutants, we find that the yields of initial $P^* \rightarrow P^+H_B^-$ ET are essentially identical and the relative higher/lower yields of $P^+Q_B^-$ derive from a rebalancing of the rate constants for the competing $P^+H_B^- \rightarrow P^+Q_B^-$ ET and $P^+H_B^-$ CR processes.

2. Material and methods

2.1. Preparation of mutants and RCs

The V(M131)X and V(M131)X+IS mutations were created in derivatives of a specifically engineered expression plasmid, pBBRKW2HTsLsM [37]. This plasmid contains strategically-placed, unique restriction enzyme sites in the L and M genes that enable rapid cassette-based mutagenesis of regions near the RC cofactors. Each V(M131)X mutation was carried on a cassette flanked by *Eco*RV and *Xma*I restriction enzyme sites and the M(M144)I–A(M145)S mutations were carried on a fragment bearing *Xma*I and *Afl*II ends. In a small subset of mutant plasmids, a synthetic cassette encoding the native Trp residue at M250 was used to replace a region flanked by unique *Nhe*I and *Nco*I sites. All mutations were verified by sequencing of candidate plasmids. RCs were expressed in *Rb. capsulatus* host strain U43 following conjugal transfer of mutant plasmids. RC expression screening and RC purification followed methods described previously [37]. Purified RCs were suspended in 10 mM Tris (pH 7.8), 0.1% Deriphat 160-C for all spectroscopic experiments.

2.2. Millisecond screening assay

The $P^+Q_B^-$ yield in the mutant RCs was determined using a dedicated apparatus of local design for studies spanning ~100 μs to ~5 min [37]. Samples, ~100 μl in volume and having $A_{865nm} = 0.05 \pm 0.005$ in a 2 mm pathlength, were arrayed and screened in 96-well plates. RCs were excited with a single ~7-ns excitation flash at 532 nm (provided by a Q-switched Nd:YAG laser) and the magnitude and decay of bleaching of the ground state absorbance of P were probed at 850 nm (provided by a continuous-wave diode laser). As controls, RCs from WT and the YFHV mutant (defined in Section 3.1) were included on every screening plate. The WT RC provides the reference of ~100% $P^+Q_B^-$ formation (from $P^+Q_A^-$) and the YFHV RC gives ~22% yield of $P^+Q_B^-$ formation via B-side ET.

2.3. Ultrafast transient absorption (TA) spectroscopy

Ultrafast TA experiments employed ~130-fs excitation and white light probe flashes at 10 Hz and an apparatus described previously [8]. Data were acquired in ~220-nm spectral windows. For experiments that probed 480–700 nm, RCs had A_{865nm} = ~0.9–1.0 (2-mm pathlength). Experiments probing 830–1050 nm utilized RCs with A_{865nm} = ~0.5–0.6 (2 mm pathlength). To ensure that fresh sample was excited on each laser flash, 2.0–2.5 ml of RCs were flowed rapidly through a 2-mm pathlength cell and an ice-cooled (~10 °C) reservoir.

2.4. Extended-timescale ultrafast TA measurements

TA measurements on the ~0.5 ns to 450 μs timescale utilized 1 kHz, ~130-fs excitation flashes at 865 nm provided by an amplified (Spitfire Ace) Ti:sapphire (MaiTai) laser system (Spectra Physics) coupled to a Topaz (Light Conversion) optical parametric amplifier. An EOS detection system (Ultrafast Systems Inc.) provided ~1 ns white light probe light flashes that are slaved to the 1 kHz clock of the ultrafast laser system. The instrument response function (if viewed as a Gaussian) of the EOS detection system is ~0.5 ns. TA spectra (400–800 nm window) were averaged into "bins" (100-ps minimum width) with 450 μs being the longest delay time possible at a 1 kHz repetition rate. RC samples used for these experiments were stirred rapidly and contained terbutryn (tb), a competitive inhibitor of Q_B binding. In particular, 10–13 μL of a

40 mM tb stock solution in ethanol was added to 0.40–0.50 ml of ~25 μM RCs to obtain a final concentration of ~1 mM tb (~40:1 ratio of tb: RCs), keeping the ethanol concentration at ≤3%. Steady-state oxidation of the samples during the 1 kHz experiments was prevented by adding ~2.5 μL of 400 mM ascorbic acid stock to give a final concentration of 2 mM.

2.5. Spectrochemical redox measurements

The P/P^+ midpoint potentials of selected mutant RCs were determined as described previously [42].

3. Results and discussion

3.1. Mutant RCs

The V(M131)X and V(M131)X+IS mutants bear a core set of mutations (Fig. 1A; Table 1) that have been shown previously to enhance B-side ET at the expense of A-side ET [8,15,37]. In the "YFHV" and "YFH" mutants that were used as templates for the insertion of the mutations at M131 and/or at M144-145, Y denotes change of the native Phe at L181 to Tyr (near B_B) and F denotes substitution of the native symmetry-related M208 Tyr to Phe (near B_A). The H designation indicates substitution of the native Leu at M212 (near H_A) with His, resulting in incorporation of a BChl (denoted β) in place of H_A [43]. This allows unambiguous spectroscopic resolution of $P^+H_B^-$ Q_x bleaching [5,8,15] in mutants chosen from the ms assay for more in-depth studies. For RCs in Deriphat/Tris, the combination of the YFH mutations provides ~40% $P^* \rightarrow P^+H_B^-$ ET, along with ~50% yield of $P^* \rightarrow P^+\beta^-$ and ~10% P^* internal conversion to the ground state [44]. The same is true of the YFHV RC, where the V designation refers to replacement of Trp at M250 by Val, a substitution that prevents RCs from incorporating Q_A [45,46]. Two of the V(M131)X+YFHV mutants did not produce RCs (Q and Y) whereas six of the V(M131)X+ISYFHV mutants failed to produce RCs (P, L, A, S, F and R).

3.2. Ground state absorption spectra of mutant RCs

Ground state spectra of the isolated RCs are shown in Fig. 2A and B. The P absorbances near 865 nm are relatively similar among the mutants, while some differences exist in the Q_x and Q_y absorbance regions of H_B. At first glance, spectra of purified RCs containing K and Y substitutions at M131 (in the ISYFHV background) appear to indicate that these RCs may lack H_B since there is no resolved 760-nm peak (Fig. 2A). In fact, the Q_y absorption of this cofactor has been red-shifted and is not resolved from the Q_y absorption of β near 780 nm [43]. The spectra of RCs containing the H and W substitutions at M131 in combination with ISYFHV have a similar appearance, but to a lesser degree (not shown). In the M131X+YFHV mutants, red-shifted Q_y absorptions for H_B are noted in the RCs carrying K, H, W, F, and R substitutions (Fig. 2A). Less pronounced are analogous spectral shifts in the set of mutants that were chosen, based on the ms assay results presented below (Section 3.3), for extensive spectroscopic characterization (Fig. 2B). Here, the substitution of E or I at M131 has limited influence on the Q_y absorption of H_B and can be seen to red-shift its Q_x absorption; this shift is more pronounced in the YFHV background relative to the ISYFHV background.

Table 1
Key mutant RC designations.[a]

RC	Mutations
WT	none
YFHV	F(L181)Y-Y(M208)F-L(M212)H-W(M250)V
ISYFHV	M(M144)I-A(M145)S-YFHV
E+YFHV	V(M131)E-YFHV
E+ISYFHV	V(M131)E-ISYFHV
I+YFHV	V(M131)I-YFHV
I+ISYFHV	V(M131)I-ISYFHV

[a] L(M212)H results in incorporation of a BChl (denoted β) in place of H_A; W(M250)V results in the absence of Q_A from the RC.

3.3. $P^+Q_B^-$ yields determined from the millisecond screening assay

The ms screening results for the yield of formation of $P^+Q_B^-$ in the sets of V(M131)X+YFHV and V(M131)X+ISYFHV mutant RCs are shown in Fig. 3 along with WT, YFHV, and W(M250)V controls. Because the mutant RCs do not bind Q_A (again, owing to the presence of the W(M250)V mutation; Table 1), the only long-lived charge-separated state that can be present is $P^+Q_B^-$ formed via B-side ET [37]. The WT RC screened in the ms assay provides the control of 100% formation of $P^+Q_B^-$ via A-side charge separation and $P^+Q_A^- \rightarrow P^+Q_B^-$ ET. The orange-filled bars in Fig. 3 give the results for RCs carrying 17 amino acids at M131 in the YFHV background. Glu at M131 (mutant E+YFHV, left-most orange bar) significantly improves the yield of $P^+Q_B^-$ compared to the native Val (control sample YFHV, yellow bar). The Asn, Gly, Asp and Ile substitutions are also better than or comparable to the native Val in promoting B-branch formation of $P^+Q_B^-$, and several other amino acids rank just slightly below Val in supporting B-side ET.

The blue-outlined (open) bars in Fig. 3 show the results of screening 15 amino acid substitutions at M131 in a background where the IS pair of mutations [M(M144)I+A(M145)S] has been added to YFHV. Compared to YFHV, the assay indicates that a higher yield of $P^+Q_B^-$ is obtained in the ISYFHV mutant RC. The same comparison holds for adding the IS mutations to the V(M131)I+YFHV construct to give mutant I+ISYFHV. For a given residue at M131, the $P^+Q_B^-$ yield goes down upon addition of the IS substitutions in about half of the cases and goes up or stays the same in half. For the four top performing residues at M131 (E, N, G, D), addition of the IS substitutions results in significantly lower $P^+Q_B^-$ yield.

3.4. Millisecond assay considerations

3.4.1. Photochemical recycling

In the ms assay, it is possible for 'recycling' of the RC photochemistry to occur when fast (ps–ns timescale) CR processes return RCs to the ground state, which can then be re-excited during the 7-ns excitation flash. For example, upon excitation $P^+\beta^-$ is formed on the A side in ~50% yield in the YFHV background (Fig. 4A). The lifetime of $P^+\beta^-$ in the absence of Q_A is ~1 ns [43,47,48] providing the opportunity for recycling. RCs that return to the ground state via P^* internal conversion (~10% yield for YFHV; Fig. 4A) may also be re-excited. Ultrafast studies have revealed that in many mutant RCs there is an ~30% 'inactive' fraction/population of P^* (discussed in Section 3.5.2) wherein P^* decays to the ground state via internal conversion in 100–200 ps; a fraction of these RCs may not be inactive on a subsequent excitation event. Because of recycling via any of these avenues, it is thus possible to obtain higher yields of charge separation in the ms assay than obtained from experiments employing ultrashort ps-fs laser flashes.

Based on the inventory of mutants screened to date and results presented here, our current assessment is that the general relative ordering of the yield of $P^+Q_B^-$ in mutant RCs is assayed reliably by the ms screen with recycling adding no more than ~10% to the measured $P^+Q_B^-$ yields. The W(M250)V mutant (Fig. 3) is a negative control that lacks Q_A but is otherwise WT. It should give no or only a very small yield of $P^+Q_B^-$ (due to a few percent inherent B-side yield, recycling, or residual Q_A content). In general, mutants with the lowest yields of $P^+Q_B^-$ formation have the greatest potential to be recycled, meaning that the poorest mutants may in fact have even lower actual $P^+Q_B^-$ yields than indicated. Conversely, the mutants with the highest yields are the least affected by recycling.

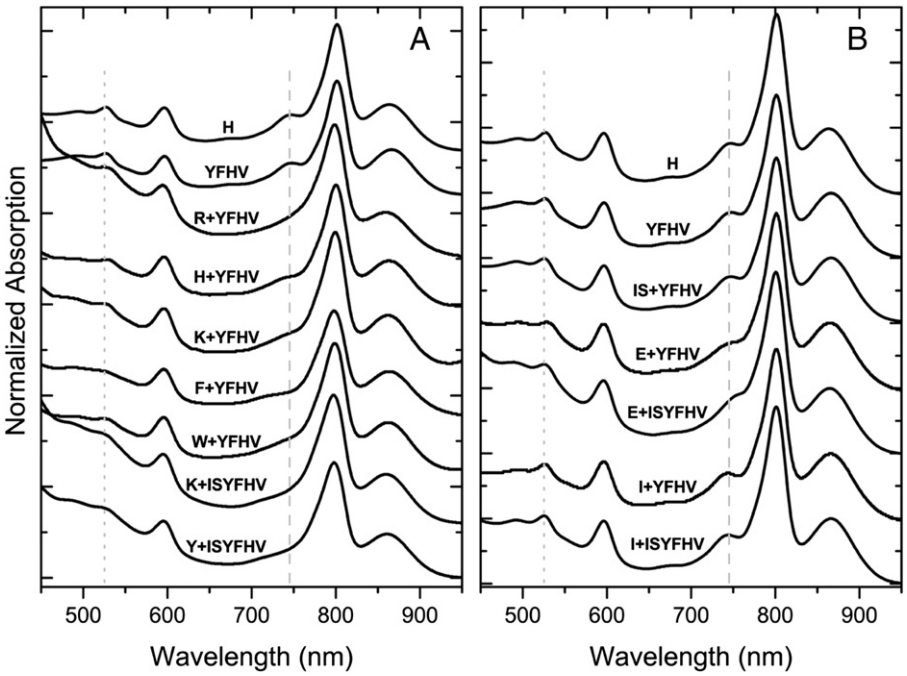

Fig. 2. Ground state spectra of RC complexes carrying mutations in the vicinity of H_B and a set of mutations (YFHV; Table 1). The spectra are for mutant RCs that are representative of the two sets generated (A) and those studied in detail (B). The spectrum of the H mutant carrying the L(M212)H substitution is given in both parts for comparison. Regions that shift with amino acid substitution are indicated by dashed (Q_y region) or dotted (Q_x region) lines.

3.4.2. Q_B occupancy

In the WT RC, after receiving two electrons from successive A-side charge-separation events and acquiring two protons, Q_B migrates out of the complex as the quinol Q_BH_2. Unlike its tightly-bound counterpart Q_A, Q_B binding is labile by natural design. We have determined that WT and YFHV control RCs have ≥90% occupancy of the Q_B site as prepared via our standard methods (Section 3.5.5). All the mutant RCs are purified similarly and the ms assay is performed on all RCs "as is" with the view that if a mutant exhibits a low yield of B-side formation of $P^+Q_B^-$, it is not considered a "hit" in our quick ms screening assay.

In optimizing and understanding our assay, however, we have explored the extent to which adding either UQ_4 or UQ_6 under a variety of conditions might increase the $P^+Q_B^-$ yield compared to the same RC with no UQ additions (i.e., prepared "as is"). In *Rb. capsulatus* RCs, both the Q_A and Q_B sites are occupied by ubiquinone-10 (UQ_{10}) molecules, which have ten repeating isoprenyl units attached to the functional headgroup; UQ_4 and UQ_6 have correspondingly fewer isoprenyl units attached to the same headgroup. A sampling of mutants has been used for this effort (ones reported here, previously, or as yet unpublished). Most of this effort has involved use of UQ_6. To date, we have not been able to discover consistent conditions for UQ_6 addition that lead to appreciable increase in magnitude of the $P^+Q_B^-$ signal in the ms assay. Nor would such readily be expected given differences in positions of mutation. In some cases, there is evidence that added quinone (UQ_4 especially) may bind in the Q_A pocket, which leads to a very undesirable false positive effect in the ms assay ($P^+Q_B^-$ that derives from ET to Q_A and subsequent ET from Q_A to Q_B).

Clearly lack of change in the amplitude of $P^+Q_B^-$ formation upon addition of quinone cannot distinguish between whether an RC has full Q_B occupancy to start with or whether the occupancy is low and exogenous quinone fails to be incorporated under the conditions tested. Depending on the site(s) of the mutation(s), knowledge of the exact occupancy of the Q_B site is needed for those mutants that score high in the ms assay and are investigated further in ultrafast studies. Such is the case here and determinations of Q_B occupancy for a subset of six mutants will be described below (Section 3.5.5) in the context of data analysis to determine the rates and yields of $P^+H_B^- \rightarrow P^+Q_B^-$ ET.

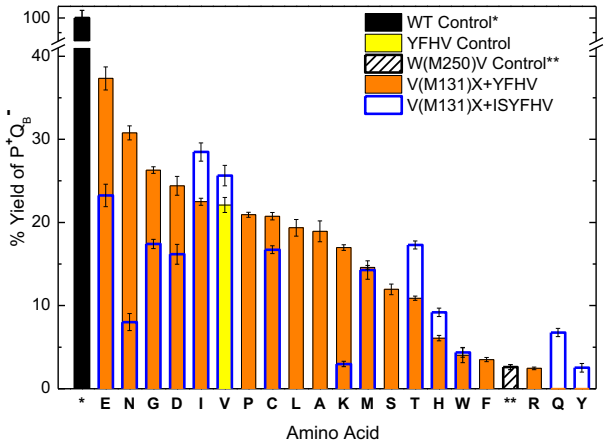

Fig. 3. $P^+Q_B^-$ yields in the V(M131)X+YFHV (orange bars) and V(M131)X+ISYFHV (blue outline bars) mutant RCs relative to controls WT (solid black bar), YFHV (solid yellow bar) and W(M250)V (black-hashed bar) obtained from the millisecond screening assay. In the WT RC, $P^+Q_B^-$ forms in 100% yield via initial A-side charge separation and $P^+Q_A^- \rightarrow P^+Q_B^-$ ET.

3.5. Ultrafast spectroscopic analysis of the six mutant RCs

Based on the ms assay results, six mutant RCs were selected for ultrafast TA studies: YFHV (the starting template mutant), ISYFHV, E+YFHV, E+ISYFHV, I+YFHV and I+ISYFHV (Table 1). The yield of $P^+Q_B^-$ in all five of the new mutants is about the same as or larger than found for YFHV (Fig. 3). The ultrafast measurements confirm this basic result and unravel changes to the properties of the B-side charge-separated states that lead to the E+YFHV mutant producing the most $P^+Q_B^-$. Analysis of the ultrafast measurements requires the considerations presented in the following subsections that ultimately lead (Section 3.5.6) to the conclusion that mutations described here

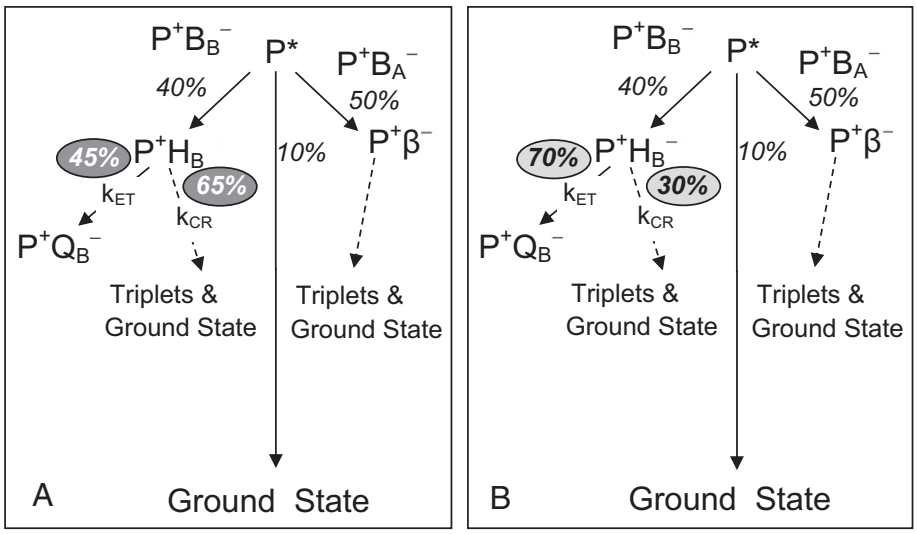

Fig. 4. Simplified schematic of processes observed in this study. (A) Photochemical scheme for the YFHV template RC. The yields in percent pertain to individual branching points as indicated and as currently estimated from this and previous work on YFHV RCs. (B) Photochemical scheme for the E+YFHV RC with increased yield of forward secondary ET. See the text and Eqs. (1)–(3) for definitions of k_{ET} and k_{CR}.

that result in an enhanced yield of $P^+Q_B^-$ primarily do so by slowing $P^+H_B^-$ CR.

3.5.1. General model for RC photochemistry

In the simplest picture (Fig. 4A), mutation(s) may alter the competition of processes/rates at two branching points to afford a higher yield of $P^+Q_B^-$. One possibility is that initial P* decay produces relatively more $P^+H_B^-$ compared to P* decay by internal conversion or by ET to the A side to form $P^+\beta^-$. The second is a more favorable biasing of $P^+H_B^- \rightarrow P^+Q_B^-$ ET over $P^+H_B^-$ CR to form the ground state or triplet excited states. For simplicity, we define k_{ET} as the rate constant for $P^+H_B^- \rightarrow P^+Q_B^-$ ET and τ_{ET} as the associated time constant (Eq. (1)). We define k_{CR} as the "effective rate constant" for the combination of all other processes by which $P^+H_B^-$ decays by CR, where τ_{CR} is the associated time constant (the 'CR lifetime') for the decay of the state in the absence of ET (Eq. (2)). When $P^+H_B^-$ can decay by both ET and CR (i.e., when Q_B is present), the lifetime of the state (τ_{HB}) is given by Eq. (3) and the associated yields by Eqs. (4) and (5).

$$\tau_{ET} = 1/k_{ET} = 1/\left(\tau_{HB}^{-1} - \tau_{CR}^{-1}\right) \quad (1)$$

$$\tau_{CR} = 1/k_{CR} \quad (2)$$

$$\tau_{HB} = 1/k_{HB} = 1/(k_{CR} + k_{ET}) \quad (3)$$

$$\phi_{ET} = k_{ET} \bullet \tau_{HB} \quad (4)$$

$$\phi_{CR} = k_{CR} \bullet \tau_{HB} \quad (5)$$

In RCs with native A-side cofactors, the routes by which $P^+H_A^-$ decays in the absence of ET to Q_A include spin rephasing in the initially produced singlet form of the $P^+H_A^-$ radical-pair state (i.e., $[P^+H_A^-]^1$) to produce the triplet radical pair (i.e., $[P^+H_A^-]^3$) and subsequent collapse (by CR) to give the triplet excited state of P (denoted P^R) in parallel to the decay of the singlet radical pair (by CR) to the ground state. Fig. 5 shows (potential) analogous processes for the B-side state $P^+H_B^-$ as well as for $P^+\beta^-$ on the A side. Analysis of the complex decay pathways and kinetics for the radical-pair states is beyond the scope of this work. However, we will show data indicating triplet excited state formation that support the model of the radical-pair dynamics depicted in Fig. 5. Otherwise, our results and discussion are framed in terms of Fig. 4, a simplified form of Fig. 5, in order to focus on general trends and differences found in the competition between k_{ET} and k_{CR} among the six mutants under study.

The relative free energies of the charge-separated states in WT RCs shown in Fig. 1B reflect a generally agreed-upon model derived in part from indirect measurements. One readily measured value that affects the free energies of the states relative to P* is the P/P^+ midpoint potential. Previous work has shown that, compared to a Phe, a Tyr at either L181 or M208 lowers the P/P^+ midpoint potential by ~25 mV [49]. Swapping FY for YF at L181/M208 in the YFH RC results in only a ~10 mV lower P redox potential compared to WT (Table 2), in agreement with prior studies on the YF mutant [49]. Since M131, M144 and M145 are not located near P, we expect that among the mutants reported here, the redox potential of P will (1) not vary significantly, and (2) not be significantly different than WT. For the five new selected mutants, the P/P^+ midpoint potentials vary between 466 ± 5 mV and 475 ± 2 mV averaging only ~15 mV lower than 488 ± 8 mV for WT (Table 2, column 2). These values are consistent with the YF-swap and only minor additional effects upon residue changes at M131 (E or I) or at M144-M145 (IS pair) are noted. Thus, for the six mutants chosen

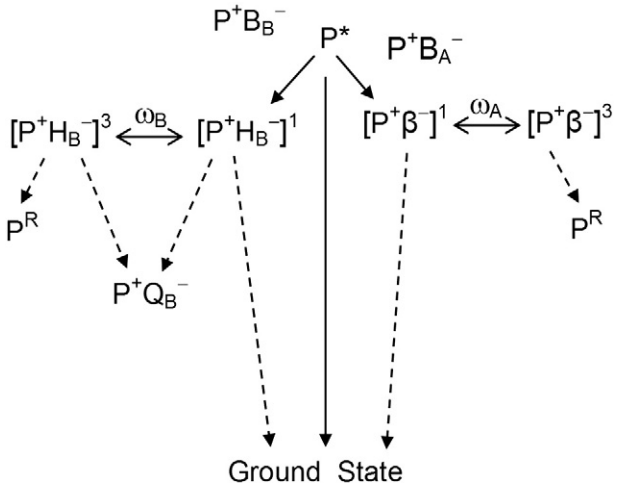

Fig. 5. An elaborated scheme of processes observed in this study for the YFHV RC that includes spin rephasing and formation of the triplet radical pair and subsequent formation of the triplet excited state of P denoted P^R.

Table 2
Properties of WT and selected mutant RCs.[a]

Sample	P Oxidation Potential (mV)	Q_B Occupancy (%)
WT	488 ± 8	94
YFH	478 ± 5	92
ISYFH	475 ± 2	90
E+YFH	469 ± 1	67
E+ISYFH	466 ± 5	47
I+YFH	471 ± 7	91
I+ISYFH	469 ± 5	78

[a] Error bars on the oxidation potentials are obtained from replicate (N ≥ 2) measurements. The Q_B occupancy has an error of ±5% of the reported value. Mutant nomenclature as given in Table 1.

Table 3
P* lifetimes and relative populations determined from stimulated emission decay.[a]

Sample[b]	τ_{P^*} 'Active' (ps)	'Active' Fraction	τ_{P^*} 'Inactive' (ps)	'Inactive' Fraction
YFH[c]	32	0.65	210	0.35
ISYFH	32	0.81	307	0.19
E+YFH	30	0.84	154	0.16
E+ISYFH	27	0.80	159	0.20
I+YFH	23	0.73	220	0.27
I+ISYFH	27	0.74	178	0.26

[a] The time constants have a typical error of ±10% of the reported value.
[b] Nomenclature for RC mutations as given in Table 1, except that these experiments were done on mutants that do not contain the W(M250)V mutant that prevents binding of Q_A.
[c] Taken from ref [44].

for ultrafast studies, the basic model in Fig. 4 is reasonably adopted. The V(M131)E mutation likely lowers the free energy of $P^+H_B^-$ by 50–100 mV (discussed in Section 3.5.6).

3.5.2. $P^* \rightarrow P^+H_B^-$ charge separation

Fig. 6 shows ultrafast TA spectra in the visible (parts A and C) and near-infrared (parts B and D) regions for RCs containing the ISYFH and E+ISYFH mutations. The TA spectra acquired 0.5 ps after excitation are identical to those obtained for WT and are assigned to P*. In the near infrared, the P* spectrum features bleaching of the long-wavelength absorption band of P at 865 nm and stimulated emission from P* extending to ~1000 nm. For all six mutants, the P* stimulated emission decay kinetics fit well to a function consisting of the instrument response plus two exponentials plus a constant. Representative data and fits are shown in the insets to panels B and D in Fig. 6. The fits can be generally summarized as revealing (1) a shorter component (~70% amplitude) ranging between 20 and 30 ps and (2) a longer component (~30% amplitude) ranging between 150 and 300 ps. For each mutant, values returned by the fits are given in Table 3, columns 2–5. In the visible region, bleaching of the Q_x band of H_B at ~530 nm in the mutant RCs develops with a time constant also in the range of 20–30 ps (Table 4, column 2), in very good agreement with the shorter of the two stimulated emission decay components (Table 3, column 2). On the other hand, the appearance (development) of bleaching of the 530 nm band of H_B does not contain a clear ~200-ps component.

Thus, the ~200-ps component found here, as found previously in many mutants, does not appear to be associated with (appreciable) charge separation but rather (primarily) with P* internal conversion to the ground state. Underscoring this analysis is a mutant in which no charge separation takes place at all and P* decays solely by internal conversion with a time constant of ~200 ps (in Deriphat; ~100 ps in LDAO) [21]. These observations are the basis of a model we have developed of 'active' and 'inactive' populations (fractions) of P*. These populations are present in ~70:30 active:inactive ratio in many (but not all) of the YF-containing mutants we have studied to date and other mutants as well [25,44,50]. These mutants have in common goals to raise the free energy of $P^+B_A^-$ (ideally placing it above P*) and lower that of $P^+B_B^-$ (ideally positioning it below P*), thereby narrowing the span of the free energies of P* and the charge-separated states and

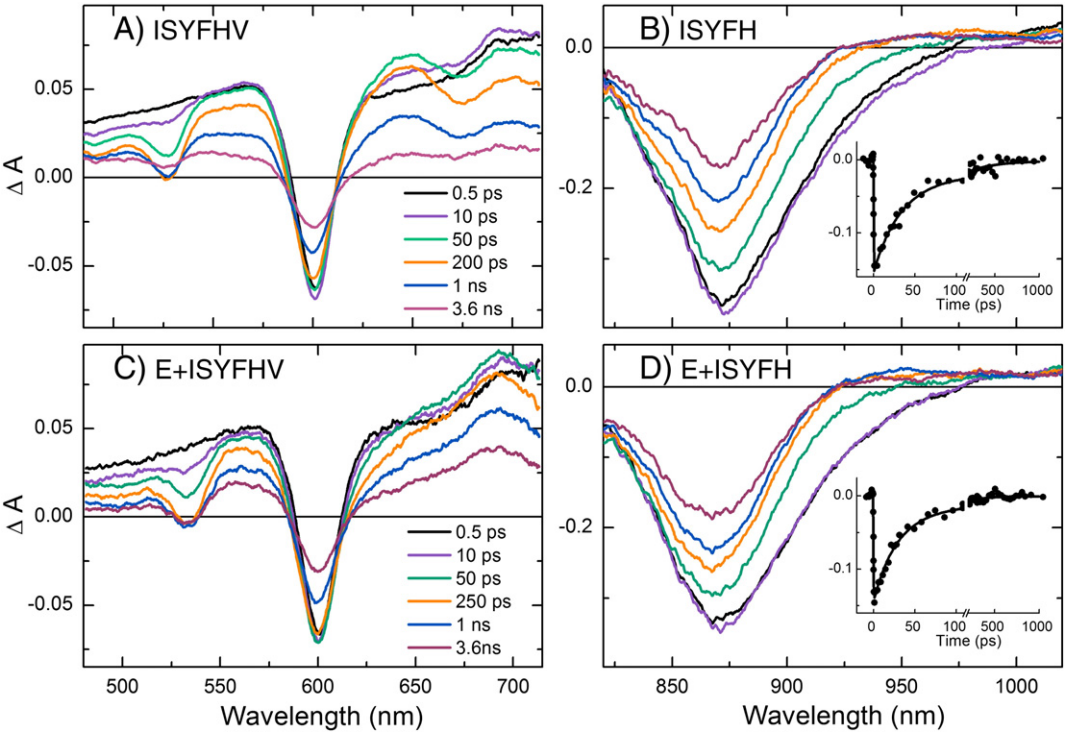

Fig. 6. TA spectra and kinetics for RCs containing the ISYFH (A and B) and E+ISYFH (C and D) mutations. The Q_x region data (A and C) were acquired at the times indicated following a 130-fs, 850-nm excitation flash. The listed times for the traces in (A) also apply to (B) and those for (C) also apply to (D). In (B) and (D) the TA spectra were acquired using 130-fs, 590-nm excitation flashes. The insets in (B) and (D) show the data (filled circles) averaged in a 10-nm interval centered on the stimulated emission isosbestic point at ~910 nm. The solid lines are a fit to the instrument response function plus two exponentials plus a constant. The presence/absence of the W(M250)V mutation has no effect on the early photochemical events.

Table 4
P* lifetime, $P^+H_B^-$ yield and position of the Q_x band of H_B in mutant RCs.[a]

Sample[b]	P* Lifetime Active Fraction (ps)	Yield of $P^+H_B^-$ (%)	H_B Q_x Bleaching (nm)
YFHV	27	46	528
ISYFHV	28	31	527
E+YFHV	29	38	534
E+ISYFHV	27	34	533
I+YFHV	23	40	527
I+ISYFHV	20	37	527

[a] Results pertain to the P* photochemically 'active' fraction. The time constants and yields have a typical error of ±10% of the reported value.
[b] Nomenclature for RC mutations as given in Table 1.

making the photochemistry more sensitive to static/dynamic effects of the protein.

The presence of a nominally inactive P* population adds a facet of complexity (another fitting component) to the data analysis procedures. With all six mutants having similar P* lifetimes in the active fraction of ~20 to ~30 ps, similar yields of $P^+H_B^-$ in the active fraction are expected. Such is found, averaging to 38% yield of $P^+H_B^-$ in the active fraction (Table 4, column 3). This value is in good agreement with those reported previously for YFH and YFHV RCs [8,44]. The results presented in this section thus show that initial $P^* \rightarrow P^+H_B^-$ ET takes place with nearly equal time constants (~70 ps) and yields (~40%) in the six mutants. (Note that this description is with respect to the P* active fraction, which will be the focus of the results and discussions from this point on, unless otherwise noted.) These results imply that the differences in $P^+Q_B^-$ yield found in the ms assay are rooted nearly entirely in the competition between $P^+H_B^- \rightarrow P^+Q_B^-$ ET versus $P^+H_B^-$ CR in the mutants, as discussed below (Section 3.5.6).

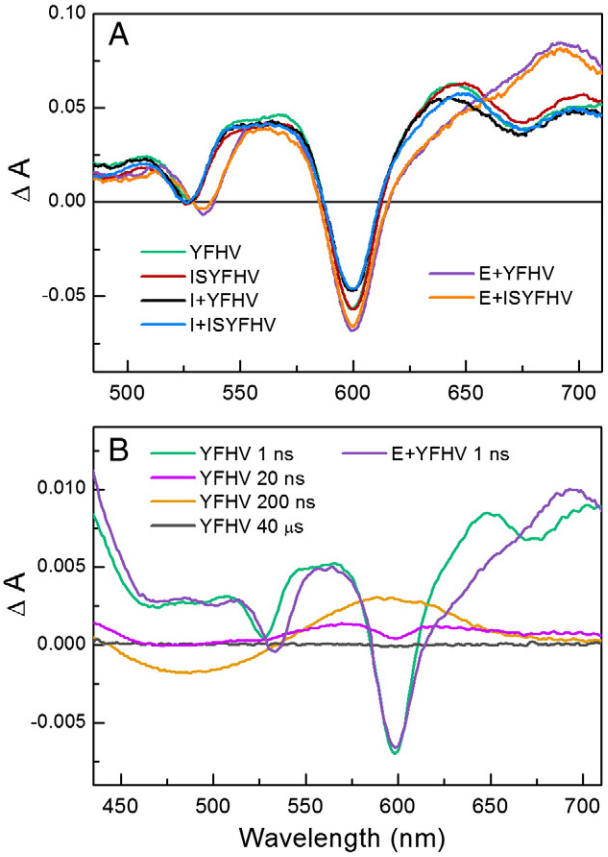

Fig. 7. (A) TA spectra of state $P^+H_B^-$ (plus a contribution of $P^+\beta^-$) comparing the ground state Q_x band bleaching and anion absorption features of H_B. The spectra were taken at roughly equivalent delay times ranging from 190–250 ps. (B) TA spectra acquired on the ns to μs timescales following a 130-fs flash at 865 nm. The spectra at 1 ns for YFHV and E+YFHV are for state $P^+H_B^-$ (plus a contribution of $P^+\beta^-$). The spectrum at 20 ns can be assigned to the triplet excited state P^R and the spectrum at 200 ns to the triplet excited state of the carotenoid (formed by energy transfer from P^R), which has a lifetime of 4.5 μs and thus has decayed completely by 40 μs.

3.5.3. Evidence that Glu (M131) forms a hydrogen bond with H_B

Fig. 7A compares matched (to the same P* amplitude at 0.5 ps) TA spectra for the six mutants. The spectra in Fig. 7A were acquired at a delay time (~200 ps) that is equal to roughly seven 1/e multiples of the lifetime of P* in the ~70% "active" fraction and one 1/e multiple of the lifetime of the ~30% "inactive" P*. Except for the two mutants carrying the V(M131)E mutation, the spectra in Fig. 7A are essentially identical to those we have reported previously at analogous delay times for YFH and YFHV RCs [8,12,37]. Since $P^+H_B^-$ lives for several nanoseconds (Section 3.5.6) these spectra largely – but not uniquely – reflect the TA spectrum of $P^+H_B^-$. There is a small contribution of the TA spectrum of P* (from the inactive P* fraction) plus TA changes due to $P^+\beta^-$ that forms on the A side in the active fraction in ~50% yield (Fig. 4). The contribution of $P^+\beta^-$ (bleaching at ~600 nm and a broad anion band between 620 and 720 nm [43,47]) "washes out" the features of a true $P^+H_B^-$ spectrum at wavelengths longer than ~610 nm that have been documented in prior studies [21]. However, the hallmark features of $P^+H_B^-$ are readily distinguished in Fig. 7A. For the YFHV, ISYFHV, I+YFHV and I+ISYFHV RCs, bleaching of the Q_x ground state absorption of H_B occurs at 527 nm (compared to the bleaching of H_A at 542–543 nm in WT) along with a relatively narrow H_B anion absorption at ~640 nm (compared to a broad absorption band for H_A at ~665 nm in WT).

The TA spectra of E+YFHV and E+ISYFHV RCs clearly differ from the spectra of the other four RCs. Both RCs containing the V(M131)E mutation reveal a 6–7 nm red shift in Q_x band of H_B, with the bleaching at 533–534 nm rather than 527 nm. The anion band absorption is positioned near 690 nm, also clearly red-shifted compared to the other four mutants. Similar but smaller shifts of these features have been reported previously for mutants with an Asp at M131, and these changes were assigned to formation of a hydrogen bond between M131Asp and the ring V keto group of H_B [10,25]. The same assertion can be made regarding the Glu substitution at M131 in the E+YFHV and E+ISYFHV mutants studied here. Interesting comparisons can be made concerning H_A and the C_2 symmetry-related residue Glu L104 on the A pathway. Glu L104 forms a hydrogen bond with H_A, which has a Q_x band at 542 nm and an anion band at 665 nm. Replacement of L104Glu by Leu removes this hydrogen bond and blue shifts the Q_x band of H_A, but not fully to the position of H_B at 527–528 nm [51,52]. (Functionally, replacing the A-side L104Glu with Leu lengthens the time constant for $P^+H_A^- \rightarrow P^+Q_A^-$ ET only slightly with no reduction of yield of $P^+Q_A^-$ reported [51].) Likewise, formation of a (putative) hydrogen bond between Glu or Asp at M131 and H_B does not reposition the Q_x absorption of H_B to that of H_A at 542–543 nm. Rather, in *Rb. capsulatus*, these two situations – the ring V keto group of non-hydrogen bonded H_A and the ring V keto group of glutamic acid-hydrogen bonded H_B – meet in the middle between 530 and 535 nm. Clearly one can invoke participation of water molecules and other differences in the local environments and global electrostatics experienced by these pigments that could affect the strengths of the hydrogen bonds [53] and/or other interactions as the causes of differences in the electronic structures and spectra of H_A and H_B.

3.5.4. $P^+H_B^-$ decay pathways in the absence of Q_B

The $P^+H_B^-$ CR pathways and dynamics were probed via ultrafast studies of the six mutant RCs to which terbutryn had been added to displace Q_B. Representative time-resolved spectra obtained using the EOS spectrometer are shown in Fig. 7B for the YFHV and E+YFHV mutants. The spectra acquired at 1 ns are largely due to $P^+H_B^-$ and have features that agree with those seen in the ~200 ps spectra in Fig. 7A obtained using standard ultrafast techniques. In particular, the V(M131)E

mutation causes a red shift in the position of both the H_B Q_x bleaching and peak of the H_B^- anion band compared to the positions of these features for the YFHV mutant.

The time evolution of the spectra in Fig. 7B not only gives a measure of the $P^+H_B^-$ lifetime in the absence of ET (~4–9 ns; Section 3.5.6) but also follows the decay pathways of $P^+H_B^-$ at longer times for the YFHV mutant. At 20 ns, the H_B bleaching at 530 nm and the H_B anion band have substantially decayed as has most of the combined P and β Q_x bleaching at ~600 nm. The 20-ns spectrum is similar to that reported previously for the triplet excited state of P (denoted P^R) in WT RCs, which forms from $P^+H_A^-$ when ET from H_A to Q_A is blocked [54], as described above (Section 3.5.1; Fig. 5). State P^R likely forms in the YFHV mutant at least in part via spin rephasing and CR from $P^+H_B^-$ and perhaps via similar events involving $P^+\beta^-$ on the A pathway. In the YFHV mutant, state P^R has a lifetime of ~100 ns and decays primarily by energy transfer to the carotenoid molecule situated near B_B (Fig. 1A), again analogous to what happens in WT RCs. The spectrum at 200 ns is assigned largely to Car^T (carotenoid triplet) and shows the expected derivative-like shape [55,56]. Car^T has an ~4.5 μs lifetime, again agreeing well with the WT RC carotenoid triplet state lifetime measured previously [55,56]. Generally similar results are found for the other five mutants investigated in detail. Further assessment of the spin rephasing events in the $P^+H_B^-$ and $P^+\beta^-$ radical pair states (Figs. 4 and 5) in the mutants is beyond the scope of this work.

3.5.5. Q_B occupancy in the six mutant RCs

Knowledge of the Q_B occupancy in the six selected mutants is a required element for determination of k_{ET} and k_{CR} (Fig. 4) via the ultrafast studies. These rate constants are readily obtained from the lifetime of $P^+H_B^-$ in the presence and in the absence of Q_B (Eqs. (1)–(3)). Determining the $P^+H_B^-$ lifetime in the presence of Q_B requires RCs in which the Q_B site is fully occupied or that we know and correct for the fraction of RCs in which Q_B is absent.

The Q_B occupancy can be assayed by the yield of $P^+Q_B^-$ formed via ET from $P^+Q_A^-$. The mutant RCs constructed for this study lack Q_A due to the presence of the W(M250)V mutation. To restore the WT Q_A binding site, allowing determination of the extent of Q_B occupancy, derivatives of the six mutant RCs under detailed study were prepared in which cassette-based mutagenesis was used to restore the native Trp residue at M250 (mutants designated E+YFH, I+YFH, ISYFH, E+ISYFH, I+ISYFH); the YFH mutant was already in hand from previous work. RCs with the native Trp at M250 are expected to contain Q_A.

$P^+Q_A^- \rightarrow P^+Q_B^-$ ET occurs with a time constant on the order of 1–100 μs and $P^+Q_B^-$ formed in this way (i.e., from the A side) decays primarily with a time constant of ~0.7 s (albeit in a pH-dependent manner along with a small-amplitude longer phase) [57,58]. If the Q_B site is not fully occupied, $P^+Q_A^-$ in the Q_B-less fraction will decay by CR to the ground state with a time constant of 100–200 ms [59]. To determine the fraction of each RC sample that is Q_B-less, the P-bleaching recovery for E+YFH, I+YFH, ISYFH, E+ISYFH, I+ISYFH, YFH, and WT RCs was assayed (using the ms screening apparatus) for detection of a 100–200 ms component. Fig. 8 shows representative data for YFH and E+ISYFH, each time profile being the average of two replications spaced ~10 min apart to allow time for excited RCs to fully recover to the ground state between excitation flashes. The data in the insets of Fig. 8 show very little of the 100–200 ms component for YFH (high occupancy of the Q_B site) and a significant 100–200 ms phase for E+ISYFH (some loss of Q_B).

The Q_B occupancy was quantitated by fitting the P-bleaching decay profiles (e.g., Fig. 8) for each of the six mutants to the sum of three exponentials and a constant. Two components within the ranges of 1.0–1.5 s and 30–40 s give consistently good fits for the bi-exponential decay of $P^+Q_B^-$. The third exponential reflects the 100–200 ms decay of $P^+Q_A^-$. For samples such as E+ISYFH with a significant Q_B-less fraction, the fits return a time constant of ~150 ms with this component being a free fitting parameter. In the case of E+ISYFH (Fig. 8B), the fits returned a relative amplitude of 0.53 for this component, indicating 47% Q_B occupancy. For samples such as YFH with very high Q_B occupancy, the fits would typically not reliably find such a low-amplitude phase so the time constant of the third component was fixed at 150 ms and the associated amplitude simply fit, yielding ≥90% Q_B occupancy in all such cases (Table 2).

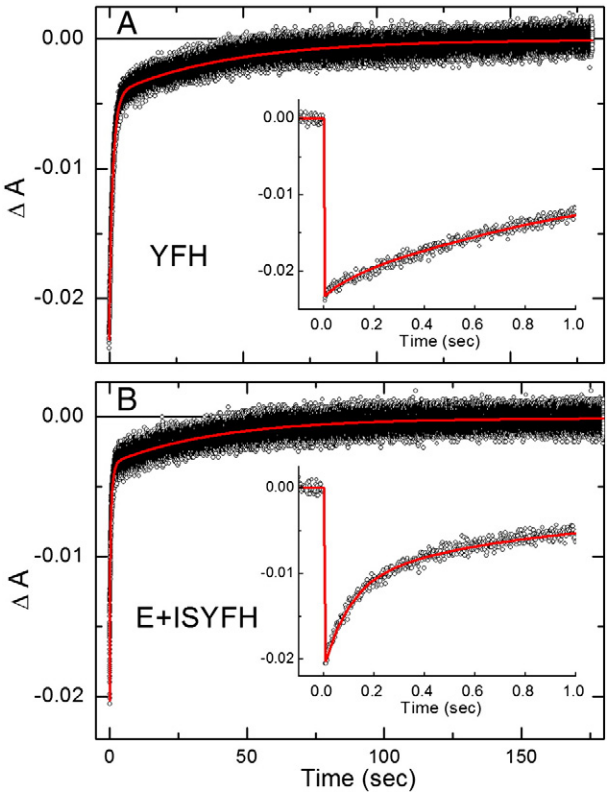

Fig. 8. P-bleaching decay profile (open circles) at 850 nm for the YFH (A) and E+ISYFH (B) RCs following excitation with a 7-ns 532-nm excitation flash. The insets show the data on an expanded scale. The solid line is a fit to a function containing three exponentials. The amplitude of the 100–200 ms component is 8% in YFH and 53% in E+ISYFH and reflects the fraction of RCs in which Q_B is absent.

3.5.6. Rates and yields of $P^+H_B^-$ decay via electron transfer versus charge recombination

The rate of $P^+H_B^- \rightarrow P^+Q_B^-$ ET (k_{ET} in Fig. 4A and B) and what we term the "effective rate" of $P^+H_B^-$ CR (k_{CR}) were determined from the $P^+H_B^-$ lifetime in the presence of Q_B (τ_{HB}) and in the absence of Q_B (τ_{CR}) (Eqs. (1)–(3)). Kinetic profiles for appearance and disappearance of bleaching of the Q_x band of H_B in all six mutants in the presence (red open circles) and absence (blue solid circles) of the Q_B-displacing terbutryn are given in Fig. 9. The H_B Q_x bleaching is at ~527 nm for YFHV, ISYFHV, I+YFHV and I+ISYFHV and is shifted to ~534 nm for E+YFHV and E+ISYFHV (see Fig. 7A). As discussed above (Section 3.5.2), as $P^+H_B^-$ forms, bleaching of the Q_x band of H_B develops with a time constant of 20–30 ps (again, reflecting the P* lifetime in the "active" fraction) in all six mutants. This signal manifests as the initial fast decrease in absorbance (i.e., appearance of bleaching) in all the kinetic traces in Fig. 9. As $P^+H_B^-$ decays, the bleaching of the Q_x band of H_B decays on the several nanosecond timescale.

Simple visual inspection of Fig. 9 shows (1) a faster $P^+H_B^-$ decay in all mutant RCs in the presence of Q_B than in its absence, and (2) much slower $P^+H_B^-$ decay for the two mutant RCs containing Glu at M131 (parts C and D). The first point reflects the obvious fact that $P^+H_B^- \rightarrow P^+Q_B^-$ ET can and does occur in the samples that contain Q_B but cannot occur when this process is inhibited by terbutryn. The second point is particularly apparent for the samples lacking Q_B (containing terbutryn)

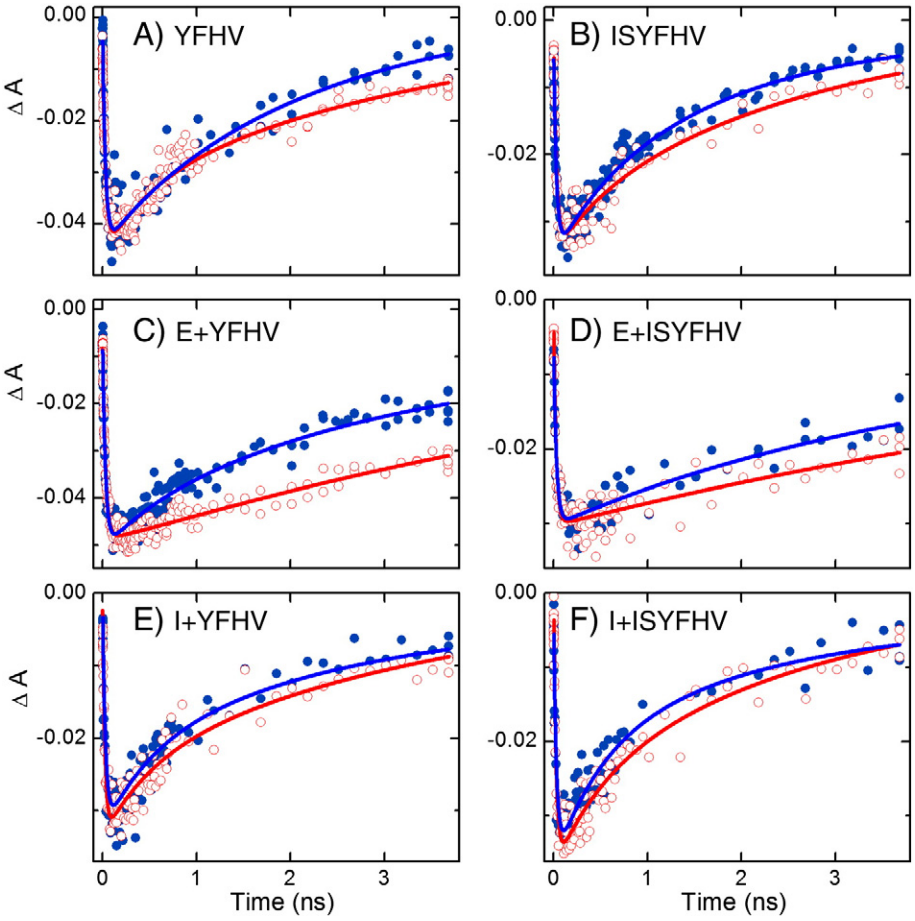

Fig. 9. Representative data (open and closed circles) and non-linear fits (solid lines), of the appearance and decay of bleaching of the Q_x band of H_B (with respect to the featureless 560–570 nm transient absorption; Fig. 7A) acquired with Q_B present at the occupancies obtained via our standard RC purification protocols (blue) and with Q_B displaced by terbutryn (red).

and qualitatively indicates that the putative hydrogen bond between H_B and Glu (M131) increases the value of τ_{CR} (and decreases k_{CR}). The second point is a major finding of this work — that the replacement of the native Val with Glu at M131 significantly slows $P^+H_B^-$ CR.

Quantifying these observations rests on obtaining the values of τ_{HB} ($P^+H_B^-$ lifetime when Q_B is present) and τ_{CR} ($P^+H_B^-$ lifetime in the absence of Q_B) and from them τ_{ET} (Eq. (1)). Determining these lifetimes has complications arising from (1) the difficult timescale involved for ultrafast TA measurements including the limited time span (~3.5 ns, Fig. 9), (2) the above-noted presence of a fraction of Q_B-less RCs in some samples, and (3) the presence of other lifetime components (e.g., decay of $P^+\beta^-$) on the same general timescale. Methodical data analysis was required to address these issues and obtain the most reliable values for comparison of the six mutant RCs. For each mutant RC, two steps to obtain τ_{CR} and τ_{HB} were performed as follows.

First, for an RC to which terbutryn has been added, the time profile of the Q_x bleaching measured by ultrafast TA (i.e., each red trace in Fig. 9) was fit with a multi-exponential function to account for the 20–30-ps decay of P* (and formation of $P^+H_B^-$), the target decay of $P^+H_B^-$, and the simultaneous decay of other states on this timescale ($P^+\beta^-$ on the A side and P* in the inactive population). The red lines through the Q_x time-profile data in Fig. 9 reflect a typical fit for each of the six mutants. Similar fitting was done for the decay of the H_B anion band at ~640 nm (for YFHV, ISYFHV, I+YFHV and I+ISYFHV) or 690 nm (for E+YFHV and E+ISYFHV). The decay profiles in the same two wavelength regions (Q_x bleaching and anion absorption) acquired by the EOS measurements provided a second type of data set with an extended time range. These data were fit similarly to a multi-exponential function that accounted for decay of the same states on the 0.1 to 100 ns time scale and the evolution of P^R and Car^T extending to many microseconds.

Table 5
$P^+H_B^-$ lifetimes and $P^+H_B^- \rightarrow P^+Q_B^-$ ET yields (Φ_{ET}).[a]

Sample[b]	$P^+H_B^-$ τ_{CR} (ns)[c]	$P^+H_B^-$ τ_{HB} (ns)[d]	$P^+H_B^- \rightarrow P^+Q_B^-$ τ_{ET} (ns)[e]	$P^+H_B^- \rightarrow P^+Q_B^-$ Φ_{ET}	$P^+H_B^-$ charge recombination Φ_{CR}
YFHV	4.0	2.2	4.9	0.45	0.55
ISYFHV	3.7	1.6	2.8	0.57	0.43
E+YFHV	9.0	2.5	3.5	0.72	0.28
E+ISYFHV	9.0	3.2	5.0	0.64	0.36
I+YFHV	4.0	1.9	3.6	0.52	0.48
I+ISYFHV	3.6	2.1	5.0	0.42	0.58

[a] The measured time constants in columns 2 and 3 have an error of ±20% of the values listed.
[b] Nomenclature for RC mutations as given in Table 1.
[c] Measured lifetime of $P^+H_B^-$ in RCs with terbutryn replacing Q_B (Eq. (2)).
[d] Measured lifetime of $P^+H_B^-$ in RCs with Q_B present (Eq. (3)).
[e] Time constant for $P^+H_B^- \rightarrow P^+Q_B^-$ ET calculated from the values in columns 2 and 3 (Eq. (1)).

The resulting best-fit values for the $P^+H_B^-$ lifetime when only CR can occur (τ_{CR}) from the two wavelength regions and the two types of data sets ("standard" ultrafast TA extending to 3.5 ns and ultrafast EOS measurements extending to many microseconds) were averaged. The resultant value is given in Table 5, column 2.

In the second step, the ultrafast TA data acquired for each mutant RC in its "as purified" condition were also fit using a multi-exponential function (blue lines, Fig. 9). Here the fitting function included an additional component accounting for the fraction of Q_B-less RCs in each sample. The time constant of this component was fixed at the τ_{CR} value derived above (Table 5, column 2) and its amplitude was fixed according to the fraction of Q_B-less RCs (Table 2, column 3). The values of τ_{HB} so determined from the decay of bleaching of the Q_x band of H_B and for the decay of the H_B anion band were averaged (Table 5, column 3). The time constant for $P^+H_B^- \rightarrow P^+Q_B^-$ ET (τ_{ET}; Eq. (1)) and the associated yields for ET (ϕ_{ET} ; Eq. (4)) and $P^+H_B^-$ CR (ϕ_{CR}; Eq. (5)) were then calculated (Table 5, columns 4, 5 and 6).

These results confirm what is apparent from examination of the raw data sets in Fig. 9 — that the inherent lifetime of $P^+H_B^-$ (decay only by CR; τ_{CR}) in the two mutants carrying the Glu substitution at M131 (E+YFHV and E+ISYFHV) is about two-fold longer compared to the four mutants that have Ile or the native Val at M131 (~9 ns versus ~4 ns). This relatively long ~9 ns 'CR lifetime' of $P^+H_B^-$ is striking and closer to the 10–20 ns lifetime of $P^+H_A^-$ in the absence of ET to Q_A. The calculated τ_{ET}, the time constant for $P^+H_B^- \rightarrow P^+Q_B^-$ ET, for the six mutants ranges between 2.8 and 5.0 ns with no clear pattern in relation to the mutations.

Comparing the mutants, it is clear that a Glu at M131 results in a significantly higher yield of $P^+H_B^- \rightarrow P^+Q_B^-$ ET than occurs when Ile or the native Val is at this position. In fact, on an absolute basis, substitution of a Glu at M131 results in a remarkable ~70% yield for this ET process (Fig. 4B), still below the roughly 100% attained on the native A side for the analogous reaction, but very high. The data in Table 5 indicate that a major, if not *the* major, origin of this result may be the hydrogen bond apparently created between M131E and H_B and significant attendant slowing of the CR processes of $P^+H_B^-$, thus allowing $P^+H_B^- \rightarrow P^+Q_B^-$ ET to compete more successfully. This result can be anticipated to be obtained in the case of other amino acid substitutions at M131 that form a hydrogen bond to H_B such as Asp and possibly Lys or His.

Many laboratories have reported significant effects on spectral, redox, photophysical, and ET properties of RC cofactors caused by the addition or removal of hydrogen bonds. Based on calculations on hydrogen bonding to the ring V group of bacteriopheophytin, and the effects of adding/removing hydrogen bonds to P in the RC [60–62], the addition of a hydrogen bond to H_B is expected to lower the free energy of $P^+H_B^-$ (stabilize the state) by as much as ~100 mV. This shift could affect the rate of CR in a number of ways, as has been discussed previously for $P^+H_B^-$ decay [12,23] and for $P^+H_A^-$ decay [28,63–67] or $P^+\beta^-$ decay [43,47,48] on the A side. Such studies suggest that the manner in which the free energy position of $P^+H_B^-$ affects its CR rate is likely more complex than simply the free energy gap from the ground state and thus the position on the (Marcus) rate versus free energy curve. Instead, this CR process, like the decay of $P^+H_A^-$ or $P^+\beta^-$ on the A side, likely involves thermal and/or quantum mechanical mixing with a higher energy state (e.g., $P^+B_B^-$) that has an inherently faster deactivation rate. The effects on ET versus CR on the A and B branches will not parallel exactly owing to specific differences, including generally higher free energies of analogous charge-separated states on the B side versus the A side, different free energy spacing of the states, and different reorganization energies.

The decrease in the rate constant for CR and the increase in the yield of ET due to the V(M131)E mutation are also accompanied by an apparent partial loss of Q_B, at least under our normal RC purification protocols. At first glance these two effects would seem to offset each other in progress towards the goal of attaining the highest possible yield of B-side charge separation to produce $P^+Q_B^-$. Yet, these results may not reflect the level of occupancy of the Q_B site when the RC is present in its native membrane environment.

3.6. Conclusions

Time-resolved spectroscopy encompassing 15 orders of magnitude was used to characterize excited-state, charge-separation and charge-recombination dynamics in a set of six RCs bearing mutations near H_B and/or Q_B. These mutant RCs are found to have similar P* lifetimes and yields of initial B-side $P^* \rightarrow P^+H_B^-$ charge separation. However, the mutations elicit varying effects on the CR lifetime of $P^+H_B^-$, the rates and yield of $P^+H_B^- \rightarrow P^+Q_B^-$ ET, and Q_B binding. Specifically, we have shown that mutation of the native Val at M131 to a Glu most likely results in formation of a hydrogen bond between the introduced Glu and H_B, as inferred from the red-shifted position of the Q_x band and anion band of H_B. Additionally, we find that a Glu at M131 slows the CR processes of $P^+H_B^-$ by a factor of two and thus boosts the yield of $P^+H_B^- \rightarrow P^+Q_B^-$ ET to ~70%.

This study shows that the balance between ET to produce $P^+Q_B^-$ and unwanted CR can be markedly improved by a single amino acid change. Interestingly, the substitution with greatest effect uncovered via saturation mutagenesis in a directed-evolution and fast-screening approach is the incorporation near H_B of a Glu at M131. This site is related by pseudo C2-symmetry to L104 that houses Glu near the photoactive H_A in the native RC. It is noteworthy that such a symmetry effect should not be viewed as an expected norm, given the many differences between the A and B sides when viewed locally or globally. For example, in a prior study focused on the first step of B-side charge separation (branched decay of P*), random mutation of sites near B_B revealed that substitutions with the greatest impact on initial ET to the B side were ionizable or polar residues [37]. Some of these residues would have been the least favored choices based on current knowledge of A-side (or B-side) architecture using a traditional site-directed approach generating select mutants one at a time. Thus, the results described herein add to those of prior work on B-side transmembrane charge separation and represent another step towards attaining a fundamental molecular-level understanding of how intricate differences in protein–cofactor interactions on the A- versus B-sides of the RC underlie differences in functionality. Such knowledge will be useful for the design of efficient, bioinspired multistep ET sequences for solar-energy conversion.

Acknowledgement

This work was supported by grant DE-FG-02-09ER16116 (to CK, DH and PDL) from DOE Office of Basic Energy Sciences, Division of Chemical Sciences, Geosciences, and Biosciences. Argonne, a U.S. Department of Energy Office of Science laboratory, is operated under Contract No. DE-AC02-06CH11357. KMF was supported by the National Science Foundation Graduate Research Fellowship under Grant No. DGE-1143954. CEZ and RJM were participants in DOE-sponsored summer internship programs for undergraduate students.

References

[1] J. Deisenhofer, O. Epp, K. Miki, R. Huber, H. Michel, Structure of the protein subunits in the photosynthetic reaction center from *Rhodopseudomonas viridis* at 3 Å resolution, Nature 318 (1985) 618–624.
[2] J.P. Allen, G. Feher, T.O. Yeates, H. Komiya, D.C. Rees, Structure of the reaction center from *Rhodobacter sphaeroides* R-26: the cofactors, Proc. Natl. Acad. Sci. U. S. A. 84 (1987) 5730–5734.
[3] C.-H. Chang, O. El-Kabbani, D.M. Tiede, J.R. Norris, M. Schiffer, The structure of the membrane-bound photosynthetic reaction center from *Rhodobacter sphaeroides* R-26, Proc. Natl. Acad. Sci. U. S. A. 30 (1991) 5352–5360.
[4] U. Ermler, G. Fritsch, S.K. Buchanan, H. Michel, Structure of the photosynthetic reaction centre from *Rhodobacter sphaeroides* at 2.65 A resolution: cofactors and protein–cofactor interactions, Structure 2 (1994) 925–936.
[5] B.A. Heller, D. Holten, C. Kirmaier, Control of electron transfer to the L-side versus the M-side of the photosynthetic reaction center, Science 269 (1995) 940–945.
[6] C. Kirmaier, D. Weems, D. Holten, M-side electron transfer in reaction center mutants with a lysine near the nonphotoactive B bacteriochlorophyll, Biochemistry 38 (1999) 11516–11530.
[7] E. Katilius, T. Turanchik, S. Lin, A.K.W. Taguchi, N.W. Woodbury, B-side electron transfer in a *Rhodobacter sphaeroides* reaction center mutant in which the B-side

monomer bacteriochlorophyll is replaced with bacteriopheophytin, J. Phys. Chem. B 103 (1999) 7386–7389.
[8] C. Kirmaier, C. He, D. Holten, Manipulating the direction of electron transfer in the bacterial reaction center by swapping Phe for Tyr near $BChl_M$ (L181) and Tyr for Phe near $BChl_L$ (M208), Biochemistry 40 (2001) 12132–12139.
[9] C. Kirmaier, P.D. Laible, K. Czarnecki, A.N. Hata, D.K. Hanson, D.F. Bocian, D. Holten, Comparison of M-side electron transfer in *Rb. sphaeroides* and *Rb. capsulatus* reaction centers, J. Phys. Chem. B 106 (2002) 1799–1808.
[10] C. Kirmaier, A. Cua, C. He, D. Holten, D.F. Bocian, Probing M-branch electron transfer and cofactor environment in the bacterial photosynthetic reaction center by the addition of a hydrogen bond to the M-side bacteriopheophytin, J. Phys. Chem. B 106 (2002) 495–503.
[11] A.L. de Boer, S. Neerken, R. de Wijn, H.P. Permentier, P. Gast, E. Vijgenboom, A.J. Hoff, B-branch electron transfer in reaction centers of *Rhodobacter sphaeroides* assessed with site-directed mutagenesis, Photosynth. Res. 71 (2002) 221–239.
[12] C. Kirmaier, P.D. Laible, D.K. Hanson, D. Holten, B-side charge separation in bacterial photosynthetic reaction centers: nanosecond-timescale electron transfer from H_B^- to Q_B, Biochemistry 42 (2003) 2016–2024.
[13] E. Katilius, J.L. Babendure, Z. Katiliene, S. Lin, A.K. Taguchi, N.W. Woodbury, Manipulations of the B-side charge-separated states' energetics in the *Rhodobacter sphaeroides* reaction center, J. Phys. Chem. B 107 (2003) 12029–12034.
[14] M.C. Wakeham, M.G. Goodwin, C. McKibbin, M.R. Jones, Photoaccumulation of the $P^+Q_B^-$ radical pair state in purple bacterial reaction centres that lack the Q_A uniquinone, FEBS Lett. 540 (2003) 234–240.
[15] C. Kirmaier, P.D. Laible, D.K. Hanson, D. Holten, B-side electron transfer to form $P^+H_B^-$ in reaction centers from the F(L181)Y/Y(M208)F mutant of *Rhodobacter capsulatus*, J. Phys. Chem. B 108 (2004) 11827–11832.
[16] M.C. Wakeham, J. Breton, E. Nabedryk, M.R. Jones, Formation of a semiquinone at the Q_B site by A- or B-branch electron transfer in the reaction center from *Rhodobacter sphaeroides*, Biochemistry 43 (2004) 4755–4763.
[17] J. Breton, M.C. Wakeham, P.K. Fyfe, M.R. Jones, E. Nabedryk, Characterization of the bonding interactions of Q(B) upon photoreduction via A-branch or B-branch electron transfer in mutant reaction centers from *Rhodobacter sphaeroides*, Biochim. Biophys. Acta 1656 (2004) 127–138.
[18] M.C. Wakeham, M.R. Jones, Rewiring photosynthesis: engineering wrong-way electron transfer in the purple bacterial reaction center, Biochem. Soc. Trans. 133 (2005) 851–857.
[19] D. Frolov, M.C. Wakeham, E.G. Andrizhiyevskaya, M.R. Jones, R. van Grondelle, Investigation of B-branch electron transfer by femtosecond time resolved spectroscopy in a *Rhodobacter sphaeroides* reaction centre that lacks the Q_A ubiquinone, Biochim. Biophys. Acta 1707 (2005) 189–198.
[20] M.L. Paddock, C. Chang, Q. Xu, E.C. Abresch, H.L. Axelrod, G. Feher, M.Y. Okamura, Quinone (Q_B) reduction by B-branch electron transfer in mutant bacterial reaction centers from *Rhodobacter sphaeroides*: quantum efficiency and X-ray structure, Biochemistry 44 (2005) 6920–6928.
[21] J.I. Chuang, S.G. Boxer, D. Holten, C. Kirmaier, High yield of M-side electron transfer in mutants of *Rhodobacter capsulatus* reaction centers lacking the L-side bacteriopheophytin, Biochemistry 45 (2006) 3845–3851.
[22] M.L. Paddock, M. Flores, R. Isaacson, C. Chang, E.C. Abresch, P. Selvaduray, M.Y. Okamura, Trapped conformational states of semiquinone (D(+center dot) Q(B)(−center dot)) formed by B-branch electron transfer at low temperature in *Rhodobacter sphaeroides* reaction centers, Biochemistry 45 (2006) 14032–14042.
[23] H.L. Kee, P.D. Laible, J.A. Bautista, D.K. Hanson, D. Holten, C. Kirmaier, Determination of the rate and yield of B-side quinone reduction in *Rhodobacter capsulatus* reaction centers, Biochemistry 45 (2006) 7314–7322.
[24] B. Carter, S.G. Boxer, D. Holten, C. Kirmaier, Trapping the $P^+B_L^-$ initial intermediate state of charge separation in photosynthetic reaction centers from *Rhodobacter capsulatus*, Biochemistry 48 (2009) 2571–2573.
[25] B. Carter, S.G. Boxer, D. Holten, C. Kirmaier, Photochemistry of a bacterial photosynthetic reaction center missing the initial bacteriochlorophyll electron acceptor, J. Phys. Chem. B 116 (2012) 9971–9982.
[26] W.W. Parson, Z.T. Chu, A. Warshel, Electrostatic control of charge separation in bacterial photosynthesis, Biochim. Biophys. Acta 1017 (1990) 251–272.
[27] T. Arlt, S. Schmidt, W. Kaiser, C. Lauterwasser, M. Meyer, H. Scheer, W. Zinth, The accessory bacteriochlorophyll: a real electron carrier in primary photosynthesis, Proc. Natl. Acad. Sci. U. S. A. 90 (1993) 11757–11761.
[28] N.W. Woodbury, J.M. Peloquin, R.G. Alden, X. Lin, S. Lin, A.K.W. Taguchi, J.C. Williams, J.P. Allen, Relationship between thermodynamics and mechanism during photoinduced charge separation in reaction centers from *Rhodobacter sphaeroides*, Biochemistry 33 (1994) 8101–8112.
[29] M. Bixon, J. Jortner, M.E. Michel-Beyerle, A kinetic analysis of the primary charge separation in bacterial photosynthesis. energy gaps and static heterogeneity, Chem. Phys. 197 (1995) 389–404.
[30] R.G. Alden, W.W. Parson, Z.T. Chu, A. Warshel, Orientation of the OH dipole of tyrosine (M)210 and its effect on electrostatic energies in photosynthetic bacterial reaction centers, J. Phys. Chem. 100 (1996) 16761–16770.
[31] M.R. Gunner, A. Nicholls, B. Honig, Electrostatic potentials in *Rhodopseudomonas viridis* reaction centers: implications for the driving force and directionality of electron transfer, J. Phys. Chem. 100 (1996) 4277–4291.
[32] A.R. Holzwarth, M.G. Muller, Energetics and kinetics of radical pairs in reaction centers from *Rhodobacter sphaeroides*. A femtosecond transient absorption study, Biochemistry 35 (1996) 11802–11831.
[33] V.A. Shuvalov, A.G. Yakovlev, Energy level of $P + B^-$ with respect to P^* found from recombination fluorescence measurements in pheophytin modified reaction centers, Biol. Membr. 15 (1998) 455–460.
[34] G. Hartwich, H. Lossau, M.E. Michel-Beyerle, A. Ogrodnik, Nonexponential fluorescence decay in reaction centers of *Rhodobacter sphaeroides* reflecting dispersive charge separation up to 1 ns, J. Phys. Chem. B 102 (1998) 3815–3820.
[35] W. Zinth, J. Wachtveitl, The first picoseconds in bacterial photosynthesis — ultrafast electron transfer for the efficient conversion of light energy, ChemPhysChem 6 (2005) 871–880.
[36] Y. Kakitani, A. Hou, Y. Miyasako, Y. Koyama, H. Nagae, Rates of the initial two steps of electron transfer in reaction centers from *Rhodobacter sphaeroides* as determined by singular-value decomposition followed by global fitting, Chem. Phys. Lett. 492 (2010) 142–149.
[37] K.M. Faries, L.L. Kressel, M.J. Wander, D. Holten, P.D. Laible, C. Kirmaier, D.K. Hanson, High throughput engineering to revitalize a vestigial electron transfer pathway in bacterial photosynthetic reaction centers, J. Biol. Chem. 287 (2012) 8507–8514.
[38] E. Nabedryk, J.P. Allen, A.K.W. Taguchi, J.C. Williams, N.W. Woodbury, J. Breton, Fourier-transform infrared study of the primary electron-donor in chromatophores of *Rhodobacter sphaeroides* with reaction centers genetically-modified at residue-M160 and residue-L131, Biochemistry 32 (1993) 13879–13885.
[39] F. Muh, J.C. Williams, J.P. Allen, W. Lubitz, A conformational change of the photoactive bacteriophyeophytin in reaction centers from *Rhodobacter sphaeroides*, Biochemistry 37 (1998) 13066–13074.
[40] W.J. Coleman, D.C. Youvan, Atavistic Reaction-Center, Nature 366 (1993) 517–518.
[41] E.J. Bylina, R.V.M. Jovine, D.C. Youvan, A genetic system for rapidly assessing herbicides that compete for the quinone binding-site of photosynthetic reaction centers, Bio/Technology 7 (1989) 69–74.
[42] M. Saggu, B. Carter, X. Zhou, K.M. Faries, L. Cegelski, D. Holten, S.G. Boxer, C. Kirmaier, Putative hydrogen bond to tyrosine M208 in photosynthetic reaction centers from *Rhodobacter capsulatus* significantly slows primary charge separation, J. Phys. Chem. B 118 (2014) 6721–6732.
[43] C. Kirmaier, D. Gaul, R. DeBey, D. Holten, C.C. Schenck, Charge separation in a reaction center incorporating bacteriochlorophyll in place of photoactive bacteriopheophytin, Science 251 (1991) 922–927.
[44] C. Kirmaier, P.D. Laible, E. Hinden, D.K. Hanson, D. Holten, Detergent effects on primary charge separation in wild-type and mutant *Rhodobacter capsulatus* reaction centers, Chem. Phys. 294 (2003) 305–318.
[45] P.D. Laible, C. Kirmaier, C.S.M. Udawatte, S.J. Hofman, D. Holten, D.K. Hanson, Quinone reduction via secondary b-branch electron transfer in mutant bacterial reaction centers, Biochemistry 42 (2003) 1718–1730.
[46] W.J. Coleman, E.J. Bylina, W. Aumeier, J. Siegl, U. Eberl, R. Heckmann, A. Ogrodnik, M.E. Michel-Beyerle, D.C. Youvan, Influence of mutagenic replacements of tryptophan M250 on electron transfer rates involving primary quinone in reaction centers of *Rhodobacter capsulatus*, in: M.E. Michel-Beyerle (Ed.), Structure and Function of Bacterial Photosynthetic Reaction Centers, Springer-Verlag, New York, 1990, pp. 273–281.
[47] B.A. Heller, D. Holten, C. Kirmaier, Effects of Asp residues near the L-side pigments in bacterial reaction centers, Biochemistry 35 (1996) 15418–15427.
[48] C. Kirmaier, L. Laporte, C.C. Schenck, D. Holten, The nature and dynamics of the charge-separated intermediate in reaction centers in which bacteriochlorophyll replaces the photoactive bacteriopheophytin. 2. The rates and yields of charge separation and recombination, J. Phys. Chem. 99 (1995) 8910–8917.
[49] Y. Jia, T.J. DiMagno, C.-K. Chan, Z. Wang, M. Du, D.K. Hanson, M. Schiffer, J.R. Norris, G.R. Fleming, M.S. Popov, Primary charge separation in mutant reaction centers of *Rhodobacter capsulatus*, J. Phys. Chem. 97 (1993) 13180–13191.
[50] J.I. Chuang, S.G. Boxer, D. Holten, C. Kirmaier, Temperature dependence of electron transfer to the M-side bacteriopheophytin in *Rhodobacter capsulatus* reaction centers, J. Phys. Chem. B 112 (2008) 5487–5499.
[51] E.J. Bylina, C. Kirmaier, L.M. McDowell, D. Holten, D.C. Youvan, Influence of an amino acid residue on the optical properties and electron transfer dynamics of a photosynthetic reaction center complex, Nature 336 (1988) 182–184.
[52] C. Kirmaier, L. Laporte, C.C. Schenck, D. Holten, The nature and dynamics of the charge-separated intermediate in reaction centers in which bacteriochlorophyll replaces the photoactive bacteriopheophytin. 1. Spectral characterization of the transient state, J. Phys. Chem. 99 (1995) 8903–8909.
[53] V. Palaniappan, D. Bocian, Resonance raman spectroscopic evidence for dielectric asymmetry in bacterial photosynthetic reaction centers, J. Am. Chem. Soc. 117 (1995) 3647–3648.
[54] W.W. Parson, R.K. Clayton, R.J. Cogdell, Excited states of photosynthetic reaction centers at low redox potentials, Biochim. Biophys. Acta 387 (1975) 265–278.
[55] T.G. Monger, R.J. Cogdell, W.W. Parson, Triplet-states of bacteriochlorophyll and carotenoids in chromatophores of photosynthetic bacteria, Biochim. Biophys. Acta 449 (1976) 136–153.
[56] J.B. Arellano, T.B. Melo, P.K. Fyfe, R.J. Cogdell, K.R. Naqvi, Multichannel flash spectroscopy of the reaction centers of wild-type and mutant *Rhodobacter sphaeroides*: bacteriochlorophll(B)-mediated interaction between the carotenoid triplet and the special pair, Photochem. Photobiol. 79 (2004) 68–75.
[57] D. Kleinfeld, M.Y. Okamura, G. Feher, Electron transfer in reaction centers of *Rhodopseudomonas sphaeroides*. I. Determination of the charge recombination pathway of $D^+Q_AQ_B^-$ and free energy and kinetic relations between the acceptor states $Q_A^-Q_B$ and $Q_AQ_B^-$, Biochim. Biophys. Acta 766 (1984) 126–140.
[58] P. Sebban, P. Maroti, D.K. Hanson, Electron and proton-transfer to the quinones in bacterial photosynthetic reaction centers — insight from combined approaches of molecular genetics and biophysics, Biochimie 77 (1995) 677–694.
[59] H. Arata, W.W. Parson, Delayed fluorescence from *Rhodopseudomonas-sphaeroides* reaction centers — enthalpy and free-energy changes accompanying electron-transfer from P-870 to quinones, Biochim. Biophys. Acta 638 (1981) 201–209.
[60] M.E. Michel-Beyerle, M. Plato, J. Deisenhofer, H. Michel, M. Bixon, J. Jortner, Unidirectionality of charge separation in reaction centers of photosynthetic bacteria, Biochim. Biophys. Acta 932 (1988) 52–70.

[61] J.P. Allen, J.C. Williams, Relationship between the oxidation potential of the bacteriochlorophyll dimer and electron transfer in photosynthetic reaction centers, J. Bioenerg. Biomembr. 27 (1995) 275–283.
[62] A. Ivancich, K. Artz, J.C. Williams, J.P. Allen, T.A. Mattioli, Effects of hydrogen bonds on the redox potential and electronic structure of the bacterial primary electron donor, Biochemistry 37 (1998) 11812–11820.
[63] K. Gibasiewicz, M. Pajzderska, J.A. Potter, P.K. Fyfe, A. Dobek, K. Brettel, M.R. Jones, Mechanism of recombination of the $P^+H_A^-$ radical pair in mutant *Rhodobacter sphaeroides* reaction centers with modified free energy gaps between $P^+B_A^-$ and $P^+H_A^-$, J. Phys. Chem. B 115 (2011) 13037–13050.
[64] K. Gibasiewicz, M. Pajzderska, A. Dobek, J. Karolczak, G. Burdzinski, K. Brettel, M.R. Jones, Analysis of the temperature-dependence of $P^+H_A^-$ charge recombination in the *Rhodobacter sphaeroides* reaction center suggests nanosecond temperature-independent protein relaxation, Phys. Chem. Chem. Phys. 15 (2013) 16321–16333.
[65] N.W. Woodbury, W.W. Parson, Nanosecond fluorescence from isolated photosynthetic reaction centers of *Rhodopseudomonas sphaeroides*, Biochim. Biophys. Acta 767 (1984) 345–361.
[66] C.-K. Tang, J.C. Williams, A.K.W. Taguchi, J.P. Allen, N.W. Woodbury, $P^+H_A^-$ charge recombination rate constant in *Rhodobacter sphaeroides* reaction centers is independent of P/P^+ midpoint potential, Biochemistry 38 (1999) 8794–8799.
[67] L. Laporte, L.M. McDowell, C. Kirmaier, C.C. Schenck, D. Holten, Insights into the factors controlling the rates of the deactivation processes that compete with charge separation in photosynthetic reaction centers, Chem. Phys. 176 (1993) 615–629.